Congresso de Métodos Numéricos em Engenharia 2015
Lisboa, 29 de Junho a 2 de Julho, 2015

MULTIOBJECTIVE DESIGN OPTIMIZATION OF CRUCIFORM SPECIMENS FOR BIAXIAL FATIGUE LOADING AS A FUNCTION OF MATERIAL AND MANUFACTERING LIMITATIONS

R. Batista[1,2], R. A. Claudio[1,2], L. Reis[2], J. F. A. Madeira[2,3], I. Guelho[2], M. Freitas[2]

1 ESTSETÚBAL, Instituto Politécnico de Setúbal, Campus do IPS, Estefanilha, 2910-761 Setúbal, Portugal.
2 IDMEC, Instituto Superior Técnico, Universidade de Lisboa , Av. Rovisco Pais, 1049-001 Lisboa, Portugal.
3 ISEL, Instituto Superior de Engenharia de Lisboa, Rua Conselheiro Emídio Navarro, 1,1959-007 Lisboa, Portugal

ricardo.baptista@estsetubal.ips.pt

Keywords: Biaxial fatigue, In-plane testing, Specimen optimization, Direct multisearch, Renard series; multiobjective design

Abstract *Cruciform specimen design, for biaxial fatigue loading applications, requires a large number of variables in order to be fully defined. Two of the most important variables are the base material thickness and the minimum center thickness that can be machined in order to reduce the specimen thickness on the gauge area. While the first one is constrained by the commercially available material sheet thickness, the second one is limited by the ability to machine the material to a minimum thickness, which is a function of the manufacturing process and the material itself. Combining this fact with the use of a new generation of biaxial fatigue testing machines, that uses quite efficient electrical motors but with limited load capacity, the cruciform specimen geometry needs to be optimized, in order to achieve the higher stress levels possible on the specimen center, while making sure the geometry is possible to manufacture. Using a cruciform geometry, with an elliptical fillet between the specimen arms and a revolved spline to reduce the specimen center thickness, a multi-objective optimization was used to achieve the optimal values for the design variables. The first objective function was defined to achieve the maximum stress level on the specimen center, which leads to fatigue crack initiation without the need for a notch. The second objective function was defined to achieve the center thickness itself, in order to avoid manufacturing problems, being necessary to have the higher value possible. Using the* Direct Multi-Search *algorithm, which is a derivate-free optimization method, a Pareto Front was obtained for each one of the base material thickness, ranging from 1 to 10 mm, defined in the Renard series of preferred numbers. In this Pareto front different optimal configurations exist and the end user can choose the applicable one for the used material and manufacturing process. Finally a full map of optimal design configurations was produced, in order to serve as a standard design procedure for cruciform specimens.*

1. INTRODUCTION

The biaxial fatigue behavior of several alloys and their main applications on industry, has been previously reported by Shanyavskiy [1], Sunder et al. [2] and Cláudio et al. [3]. Recently different types of specimens and biaxial fatigue testing machines have been developed by the scientific community and therefore new challenges must be solved in order to assess the mechanical properties. Using the latest generation of in-plane biaxial fatigue testing machines, like the one developed by Cláudio et al. [4], using smaller and more efficient electrical motors, requires new specimens, with an optimal geometry, allowing to attain higher stress levels using lower loads. The cruciform specimen is used for in-plane testing but unlike other specimens there is still no design standardization procedure, Baptista et al. [5].

The two major challenges presented when developing a cruciform geometry for fatigue testing, either for metal alloys or composite materials, are how to reduce the stress concentration at the specimen arms and how to guaranty that the maximum stress level occurs on the specimen center and not at the specimen arms. Hanabusa et al. [6], have used slits on the specimen arms, in order to reduce the stress concentration and also to create a more uniform stress and strain distribution in the specimen center, which is also necessary to accurately determine the fatigue initiation life and the crack propagation life. Müller et al. [7] and Lamkanfi et al. [8], on the other hand have developed and tested different types of notches on the specimen arms corners in order to reduce the stress concentration and to transfer the maximum stress level to the specimen center. The solution for the second challenge is normally achieved by reducing the specimen thickness on the specimen center. Łagoda et al. [9] have successfully used a revolved arc, with a large radius, to achieve a higher stress level on the specimen center, and Bonnand et al. [10] used a revolved spline on the specimen center in order to also reduce the stress concentration on the geometry change area.

In order to reduce the specimen thickness one must machine or use a metal forming process. These processes are limited by the material behavior and by other process parameters, before machining defects are introduced on the specimen or local necking or fracture appears and the final fatigue behavior is altered. Therefore there will be a minimum thickness that is possible for any combination of material and manufacturing process. Zadpoor et al. in [11] have studied the limits of aluminum alloys machinability, in terms of the minimum thickness of the reduced area. While in [12] the specimen reduced thickness and specimen thickness ratio r has been used to characterize the material machinability. On the other hand Leotoing et al. [13], have studied the material formability limits by designing and optimizing cruciform specimens.

In the current paper a cruciform specimen geometry design is optimized for the use with low capacity test machine [4], using the Direct Multi-Search (DMS) methodology to obtain several Pareto Fronts relating to two objective functions: a) maximizing the stress level on the specimen center; b) maximizing the specimen center reduced thickness. Therefore for each specimen thickness, defined by the Renard Series of preferred numbers, a list of optimal specimens will be produced as a function of the specimen center reduced thickness. All the cruciform specimens has a shape with reduced center thickness and elliptical fillet on the arms corners in order to drive the optimization process.

2. MATERIAL AND METHODS

2.1. Cruciform Specimen Design

The cruciform specimen geometry used, on Figure 1, has been previously developed by the authors [5]. This geometry is used for fatigue life initiation tests, and therefore the main goal of the specimen's features is to guarantee that the maximum stress level on the specimen occurs on the specimen center. It is also very important to achieve a uniform strain distribution on the specimen center, in order to provide the necessary conditions for fatigue initiation. As a non-uniform strain distribution will influence the fatigue life initiation, reducing this period, [14], [15] and [16].

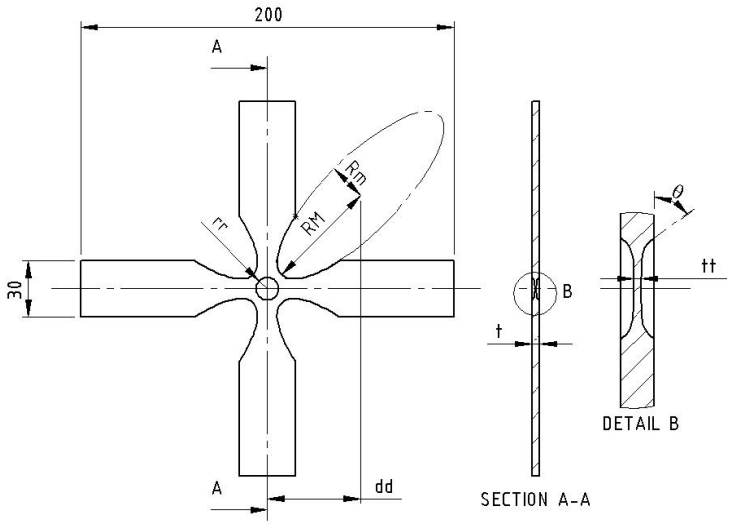

Figure 1. Specimen geometry, dimensions in mm.

This shape is based on a cruciform geometry, where the center thickness is reduced using a revolved spline, and uses an elliptical fillet in order to reduce the stress concentration in the arms corners. Using an elliptical fillet has been shown by the present authors, [5] and [17], that reduces the stress concentration on the specimen arms corners, therefore reducing the maximum stress level in this area of the specimen. Using a revolved spline, with a zero degree of tangency at the specimen center, has also been proven by the authors, [5], that increases the stress level on the specimen center, while guaranteeing a smooth and uniform strain distribution on the specimen center. The spline is also characterized by an exit angle which can be used to reduce the stress concentrations outside of the specimen center. Therefore both these features contribute to achieve the higher stress level possible on the specimen center, while maintain the strain distribution uniform under reasonable limits, at least in a radius of 1 mm, [5].
In this paper the present authors have further developed the specimen model, adding more

control over the spline definition and of course the final result. As shown in Figure 2, the spline was defined in ABAQUS using two exit angles (the angle at the center is always constant) and two dimensions (the reduced center thickness and the spline radius). Still the final form of the spline can be controlled. The authors used a tangent axis to fully define the spline form, as seen on Figure 2.

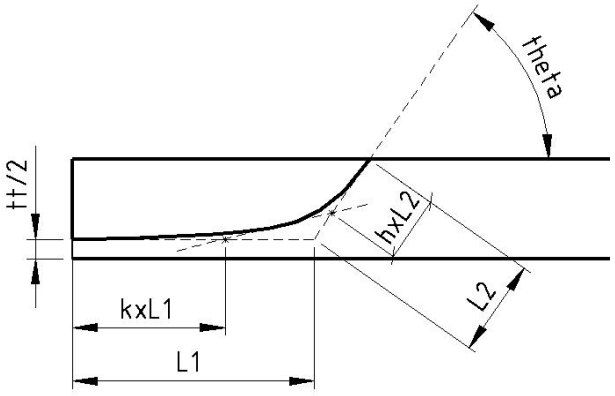

Figure 2. Close detail of the revolved spline definition.

While the spline must be tangent to this axis, the axis position can be controlled by two points, allowing to change the area were the specimen thickness is reduced. These two points are defined by two parameters and are functions of the line segments lengths, which result from the specimen geometry definition.
This geometry is defined by a total of eleven dimensions (Figs. 1 and 2). Two of them were considered constant, the specimen arm length with a value of 200 mm and the specimen arm width with a value of 30 mm for finite element modelling purposes. The main variable is the specimen thickness (t), this variable represents the chosen material sheet thickness by the end user, and is available from predefined tables accordingly to the manufacture. In the industry it is common to use the Renard Series of Preferred Numbers, [18], to define the available sheet thickness. Using this series, Table 1, presents the used values for the t variable on the present work. They follow one of the mostly used simplified forms of Renard series of preferred numbers.

R10″	**1**	**4**	**6**	**7**	**8**	**10**
Specimen thickness (t) [mm]	1.00	2.00	3.00	4.00	5.00	8.00

Table 1. Values used for the material thickness variable t.

Table 2 shows the design variables used in the optimization and the intervals used to define the optimization problem. The center thickness (tt) is the minimum thickness of the specimen, it can be considered as a function of the material and machinability capabilities, as it may be impossible to reduce the specimen thickness beyond certain values. The authors' previous works always considered this variable to be constant, but in the present

paper it is also considered to be one design variable and also one of the optimizations goals. The spline exit angle (theta) is a very important variable ensuring a smooth geometrical transition to avoid stress concentration in the critical region. The center spline radius (rr) defines the area where the specimen thickness is reduced, using the above referenced revolved spline, that has a tangency of 0º at the center. The elliptical fillet is centered between the specimen arms and is defined by three variables, the major ellipse radius (RM), the minor ellipse radius (Rm) and the ellipse center (dd). Finally two new parameters were used to fully define the spline, a parameter k and a parameter h that place the tangent axis to the spline on the optimal position. These parameters are able to change the stress level on the specimen center, but also to increase or decrease the area where the strain distribution is uniform. They act by changing the spline geometry, increasing or decreasing the area where the spline is tangent to the center and exit line segments.

	Center thickness (tt)	**Spline exit angle (theta)**	**Center spline radius (rr)**	**Major ellipse radius (RM)**	**Minor ellipse radius (Rm)**	**Ellipse center (dd)**	**Spline Parameter k (k)**	**Spline Parameter h (h)**
Min	10% of t	10º	5 mm	56 mm	16 mm	46 mm	0.3	0.7
Max	20% of t	90º	10 mm	70 mm	30 mm	60 mm	0.7	0.8

Table 2. Design variables used in the specimen design geometry optimization.

2.2. Multi-Objective Optimization

A constrained nonlinear multio-bjective optimization MOO can be mathematically formulated as, [19]:
Regarding n design variables:

$$x = (x_1, x_2, \dots x_n)^T \tag{1}$$

which minimizes:

$$min_{s,t,x\in\Omega} F(x) \equiv \left(f_1(x), f_2(x), \dots f_k(x)\right)^T \tag{2}$$

involving k objective functions $f_j: \Omega \subseteq \mathbb{R}^n \to \mathbb{R} \cup \{+\infty\}, j = 1, \dots, k$ to minimize.
Recall that to maximize f_j is equivalent to minimize $-f_j$.
$\Omega \subseteq \mathbb{R}^n (\Omega \neq \emptyset)$ represents the feasible region.
Any or all functions $f_j, j=1,\dots,k$ can hold a nonlinear nature. In general, since in MOO there are often conflicting objectives for each objective function, the concept of Pareto dominance is used to characterize global and local optimality, [19].A feasible solution of x is called a Pareto optimal if there exists no other feasible solution y such that $f_i(y) \leq f_i(x)$ for all $i=\{1,2,\dots,k\}$ with $f_j(y) < f_j(x)$ for at least one j, $j \in \{1,2,\dots,k\}$.
The Direct MultiSearch (DMS) algorithm [19] is a derivative-free method for multiobjective optimization problems. This algorithm does not aggregate or scalarize any components of the objective function and it is inspired by the search-poll paradigm of direct-search methods of directional type from single to multiobjective optimization. Through the

use of the concept of Pareto dominance, this algorithm generates and maintains a list of feasible nondominated points from which it iterates and chooses new poll centers. The DMS algorithm tries, however, to capture the whole Pareto dominance front from the polling procedure and at each iteration, if improvement is found, the new feasible evaluated points are added to the list (approximating the Pareto front) and the dominated ones are removed. Successful iterations then correspond to changes in the approximation of the Pareto front meaning that a new feasible nondominated point was found, otherwise, the iteration is declared as unsuccessful. The search step is optional and set as to best fit to the optimization problem characteristics in order to improve the numerical performance.

3. CALCULATION

3.1. Optimization Procedure

In order to perform the necessary optimization three different programs were used. Considering a single specimen thickness (t), initially MATLAB creates an input file with the values of the design variables, Table 2, for the first optimization iteration. With this file a PYTHON script creates an ABAQUS input file containing all the necessary information to run the two load cases considered. After ABAQUS has finished running the simulation the same PYTHON script extracts all the necessary information to calculate the two objective functions, using equations (3) and (4):

$$f_1(x) = -\sigma_{Maximum\ Von\ Mises\ Stress\ on\ Specimen\ Center} \tag{3}$$

$$f_2(x) = -tt \tag{4}$$

The first objective function is the negative value of the maximum Von Mises stress on the specimen center, and the second objective function is the negative value of the specimen reduced center thickness (tt). Finally MATLAB uses the DMS algorithm described above, to calculate a new set of design variables, and by repeating this procedure the Pareto Front is generated. When an adequate number of points on the Pareto Front is obtained, the procedure is restarted for a new specimen thickness (t).

While the goal of the first objective function, equation (3), is to maximize the stress level on the specimen for the available design loading capacity. The goal of the second objective function, equation (4), is to maximize the used specimen reduced center thickness (tt). In previous works, R. Baptista et al. [5], have concluded that this design variable dominates the stress optimization problem. If one considers tt as a normal design variable, it will always assume the lowest value possible. Therefore by also considering tt as an objective function, and by maximizing its value, it is possible to obtain in a single optimization problem a Pareto Front where optimal solutions for different specimen reduced center thickness exists.

3.2. Optimization Constraints

In DMS, constraints are handled using an extreme barrier function, equation (5):

$$F\Omega(x) = \begin{cases} F(x)\ if\ x \in \Omega \\ (+\infty, \dots, +\infty)\ otherwise \end{cases} \quad (5)$$

Which means that if a point is infeasible (not belonging to the predetermined feasible points universe or compromised by the problem constraints), the components of the objective function F are not evaluated and the values of F are set to +∞. This approach allows us to deal with black-box type constraints where only a yes/no answer is returned.
In the present work, the following constraints were considered, equations (6) to (9):

$$F\Omega_1(x) = \frac{\sigma_{Maximum\ on\ Center} - \sigma_{Minimum\ on\ Center}}{\sigma_{Maximum\ on\ Center}} > 10\% \quad (6)$$

$$F\Omega_2(x) = \frac{\sigma_{Maximum\ on\ Center} - \sigma_{Maximum\ on\ Inner\ Arm}}{\sigma_{Maximum\ on\ Center}} > 20\% \quad (7)$$

$$F\Omega_3(x) = \frac{\sigma_{Maximum\ on\ Center} - \sigma_{Maximum\ on\ outer\ arm}}{\sigma_{Maximum\ on\ Center}} > 20\% \quad (8)$$

$$F\Omega_4(x) = \frac{\varepsilon_{Maximum\ on\ Center\ (1mm)} - \varepsilon_{Minimum\ on\ Center\ (1mm)}}{\varepsilon_{Maximum\ on\ Center\ (1mm)}} < 2\% \quad (9)$$

Equation (6) force the solution to have a difference between the maximum and minimum stress level on the center of the specimen to be higher than 10%, while equations (7) and (8) force the solution to have a difference between the maximum stress level on the specimen center and the maximum stress level on the inner and outer portions of the specimen arms to be higher than 20%. Finally equation (9) force the solution to have a uniform strain distribution in a 1 mm radius of the specimen center, with a maximum and minimum strain difference lower than 2%. Therefore the conditions to guaranty that the fatigue initiation will occur on the specimen center and that the fatigue initiation life is not influence by any stress concentration, are satisfied.

3.3. Load Cases and Boundary Conditions

The optimization process used a simplified version of the cruciform specimen for FEM calculations. Due to symmetry, 1/8 of the geometry was modeled and symmetry boundary conditions were applied to all three symmetry planes. In a total 32315 tridimensional linear elements were used, with 40548 nodes per simulation. Also two different load cases were studied, the first load case is an in-phase (δ=0º) loading, with a 1 kN load applied in both directions. The second load case is an out-of-phase (δ=180º) loading, with a 1 kN load applied on one direction and a – 1 kN load applied to the second direction. The load is unitary in the order of magnitude of the load capacity of the actual electrical driven fatigue test machines. The chosen material is an aluminum alloy with Young modus of 69 GPa and Poisson ratio of 0.3.

4. RESULTS

4.1. Pareto Fronts

With this innovative optimization procedure, several Pareto Fronts were obtained, Figure 3a). Each Pareto Front represent all the optimal solutions obtained for each of the specimen

thickness (t) considered. The first objective function maximizes the stress level on the specimen center, while the second objective function maximizes the used specimen reduced center thickness (tt). Therefore for each value of t, different solutions were obtained as a function of tt. Organizing the solutions by value of t, one can see on Figure 3b) that the range of optimal solutions increases with t. For t equals to 1 mm, the solutions ranges from 0.14 mm to 0.16 mm of specimen reduced center thickness. As t increases to 2 mm the solutions range increases to 0.20 – 0.30 mm, for t = 3 mm the solution range is 0.30 – 0.51 mm, for t = 4 mm the solution range is 0.41 – 0.65 mm, for t = 5 mm the solution range is 0.50 – 0.77 mm and for t = 8 mm the solution range is 1.02 – 1.25 mm. The previous ranges are very important because some materials have manufacturing constraints that will limit the ability to produce a specimen with the lowest value of tt. The present results enable the specimen designer to choose a higher value of tt, which matches the required constraints, but still enables the specimen to achieve an optimal value of maximum stress.
Figure 3a) also shows that a clear relationship between the specimen reduced center thickness (tt) and the maximum stress level on the specimen center. It is clear that the stress level increases as the tt value decreases. This relation is almost independent of the specimen thickness value.

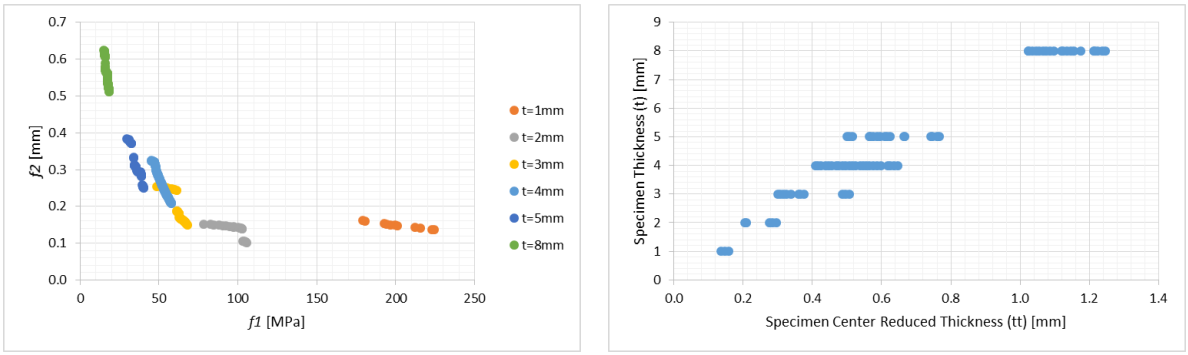

a) b)

Figure 3. a) Pareto Fronts for the different specimen thickness, b) Distribution of the obtained optimal center reduced specimen thickness.

4.2. Specimen Optimization Results

From the Pareto Front on Figure 3a) a full map of optimal design configurations was produced, Table 3, in order to serve as a standard design procedure for cruciform specimen design. This table is organized by the specimen reduced center thickness and specimen thickness ratio (r). On the optimizations problems solved r ranges from 0.1 to 0.2, and different solutions were obtained in order to satisfy different material manufacturing limitations.
In previous works [5], the authors were able to obtain only one solution for each value of t, now several solution were obtained, and it is possible to choose between them as a function of the desired value of tt. As mentioned above the solution range increases with the values of t.

Specimen thickness (t) [mm]	Major ellipse radius (RM)	Minor ellipse radius (Rm)	Spline exit angle (theta)	Center spline radius (rr)	Ellipse center (dd)	Spline Parameter k (k)	Spline Parameter h (h)	Center thickness (tt)	Maximum Stress [MPa/kN]	r=tt/t
1	63.9	22.8	90	6.5	51.3	0.50	0.71	0.137	225	0.14
1	63.4	23.0	55	6.7	51.3	0.47	0.73	0.147	201	0.15
1	63.1	23.0	32	6.5	51.3	0.49	0.72	0.159	181	0.16
2	63.4	23.0	90	9.7	53.0	0.35	0.70	0.209	104	0.10
2	63.4	23.0	87	9.7	53.0	0.35	0.70	0.213	103	0.11
2	63.4	23.0	90	7.5	51.6	0.33	0.71	0.284	101	0.14
2	63.2	23.0	90	7.5	51.6	0.33	0.71	0.291	97	0.15
3	63.0	23.0	86	10.0	53.0	0.33	0.71	0.314	66	0.10
3	63.0	23.0	83	10.0	53.0	0.33	0.71	0.316	66	0.11
3	63.4	23.0	27	10.0	53.0	0.40	0.71	0.373	62	0.12
3	63.4	23.0	26	10.0	53.0	0.40	0.71	0.375	61	0.13
3	63.0	23.0	21	8.1	51.4	0.50	0.73	0.488	61	0.16
3	63.0	23.0	21	8.1	51.7	0.50	0.73	0.497	57	0.17
4	63.0	17.8	27	8.1	51.3	0.50	0.80	0.409	58	0.10
4	63.0	18.0	26	8.1	51.3	0.50	0.80	0.428	57	0.11
4	63.0	18.9	26	8.1	51.3	0.50	0.80	0.463	55	0.12
4	63.0	19.9	26	8.1	51.3	0.50	0.80	0.500	53	0.13
4	63.0	21.3	26	8.1	51.3	0.51	0.80	0.541	51	0.14
4	63.0	22.2	26	8.1	51.3	0.51	0.80	0.581	49	0.15
4	63.2	22.5	26	7.8	51.3	0.53	0.80	0.620	48	0.16
5	63.0	22.7	90	9.9	53.0	0.34	0.70	0.502	40	0.10
5	63.0	22.7	45	9.7	52.6	0.42	0.70	0.572	39	0.11
5	63.0	22.8	45	9.7	52.6	0.42	0.70	0.576	39	0.12
5	63.0	23.0	43	9.9	53.0	0.41	0.70	0.625	34	0.13
5	63.7	23.0	34	8.6	52.8	0.46	0.73	0.742	33	0.15
8	69.5	26.7	88	9.8	58.5	0.30	0.70	1.023	18	0.13
8	69.5	26.7	88	9.8	58.6	0.30	0.70	1.081	18	0.14
8	69.1	28.1	85	9.5	58.5	0.30	0.70	1.213	16	0.15
8	69.1	28.5	85	9.5	58.6	0.30	0.70	1.241	15	0.16

Table 3. Optimal specimen geometry for different specimen thickness and specimen reduced center thickness.

5. DISCUSSION

5.1. Influence of the Specimen Thickness

If one uses the specimen thickness (t) to organize the results, one can establish a clear relationship between the design variables and the value of t for all the values of the ratio r. In Figure 4a) one can see that the value of the major ellipse radius ranges from 63 to 64 mm for values of t lower than 5 mm and then increases to around 69 mm when t is 8 mm. On Figure 4b) one can also see that the minor ellipse radius also increases with t, except for t = 4mm when the value of r is low. The value of the ellipse center, also increases when t is higher than 4 mm, Figure 4c). Therefore as t increases the elliptical fillet will increase in size and will be further away from the specimen center.
While one can see on Figure 4e) that the spline center radius increases with t for values of r higher than 0.14, there is no clear relation between the spline exit angle and the value of t, Figure 4d). R. Baptista et al. [5] have previously justified this behavior. In the present work the spline parameters h and k were used in order to try to achieve a better behavior for the spline exit angle, but as one can see on Table 3, the results were not satisfactory.
Finally on Figure 4f) one can see that the maximum stress levels are independent of the ratio r value. This is very important, as it means that the material manufacturing constraints, can be overcome by choosing a different optimal solution on Table 3, without sacrificing the maximum stress level on the specimen.

5.2. Influence of the Specimen Center Reduced Thickness and the Specimen Thickness Ratio

If one organizes the results using the value of the ratio r, the relationship between the design variables and r becomes even clearer. Figure 5a) shows the relationships between the major ellipse radius and the value of r. One can see that the general tendency is for the value of RM to be constant or to decrease with r. On Figure 5b) one can see that the values of the minor ellipse radius are constant with r, or increase with r, for the 4 mm and 8 mm thickness specimens. The ellipse center is also almost independent of the value of r, Figure 5c), so the elliptical fillet is expected to be almost constant or to increase in size for some of the specimen thickness values.
Now Figures 5d) and 5e) show a clear relation between the revolved spline geometry and the value of r. For the majority of the configurations the spline geometry will be constant, but for a specimen thickness of 3 mm and 5 mm, both the spline exit angle and the center spline radius will decrease with r.
Finally Figure 5f) shows that the final maximum stress level on the specimen is not dependent on the value of r, as only for the lowest value of the specimen thickness (t) the stress level decreases with the value of r.

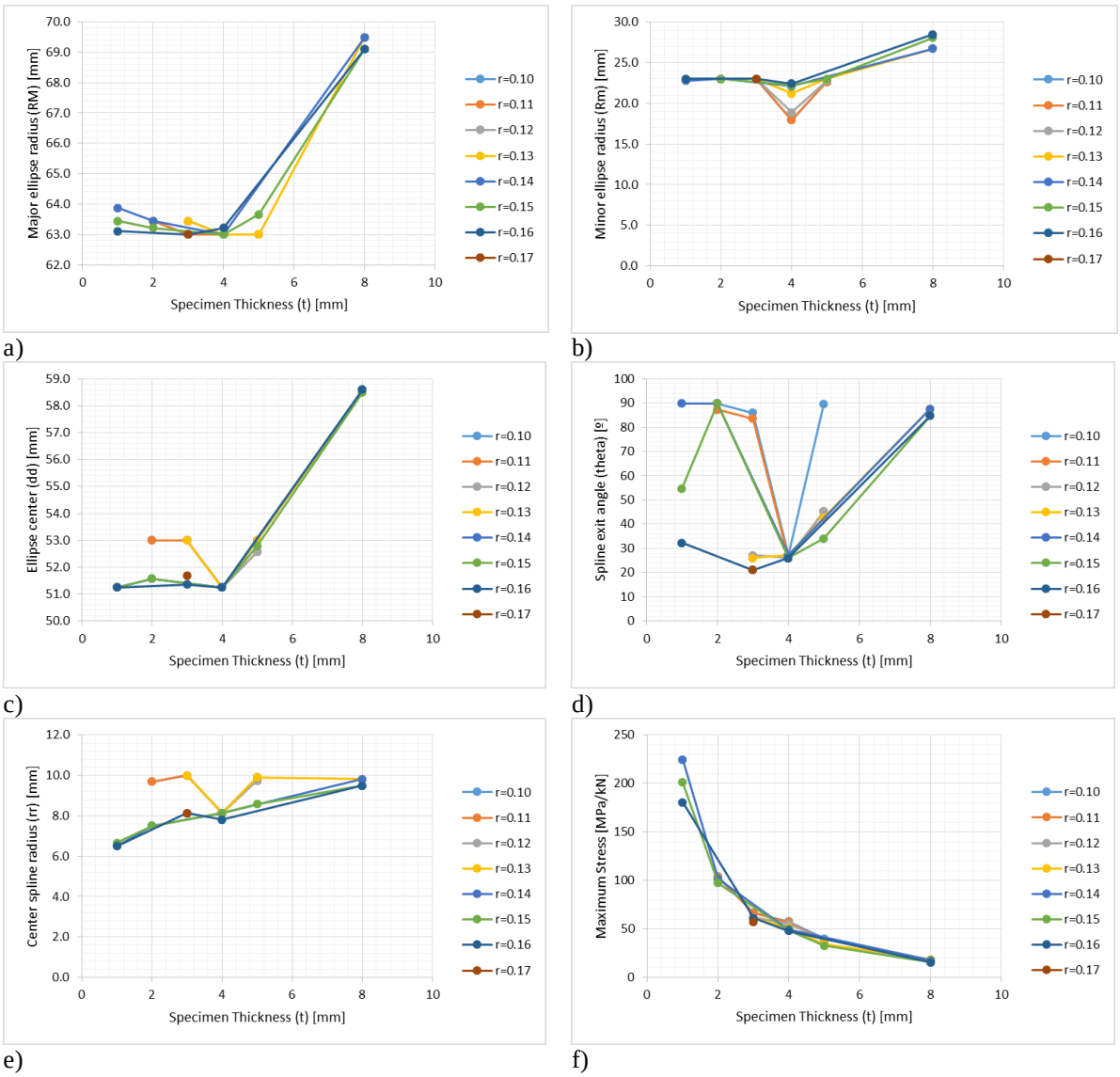

Figure 4. Design variables and maximum stress variation as a function of the specimen thickness, a) Major ellipse radius, b) Minor ellipse radius, c) Ellipse center, d) Spline exit angle, e) Center spline radius, f) Maximum Stress.

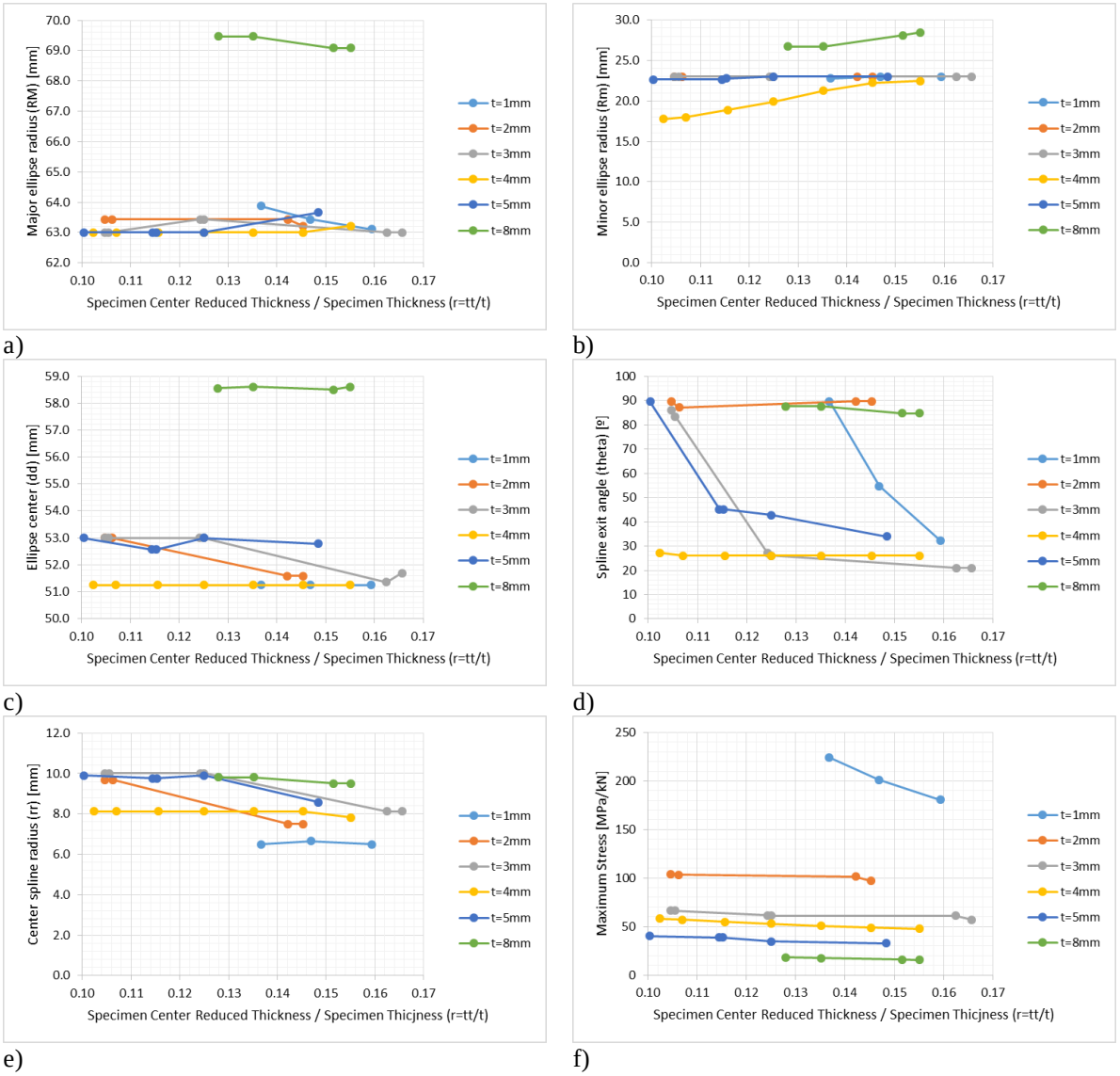

Figure 5. Design variables and maximum stress variation as a function of the specimen center reduced thickness and specimen thickness ratio, a) Major ellipse radius, b) Minor ellipse radius, c) Ellipse center, d) Spline exit angle, e) Center spline radius, f) Maximum Stress.

5.3. Strain Distribution on the Specimen Center

Previously, [5], the strain distribution on the specimen center has been target of the optimization procedure. In the present work this has not been the case, therefore the final distribution uniformity must be analyzed. Figure 6a) shows the strain distribution on a 4 mm radius around the specimen center, for different values of t. One can see that the value of t has almost no influence on the strain distribution evolution, except for the 4 mm thickness specimen. For all the other configurations the maximum strain difference on a 1 mm radius around the specimen center was 0.21%. While for t = 4 mm the maximum strain difference is 1.35%. All the values

are of course lower than the 2% imposed limit.
On the other hand, Figure 6b), shows that the ratio r has a clear influence on the strain distribution on the specimen center. It is possible to calculate that the maximum strain difference on a 1 mm radius increases from 0.37% to 1.31%, as the ratio r increases from 0.10 to 0.17. This behavior is justified by the final revolved spline geometry, which has been demonstrated to be very important on the strain distribution, [5].

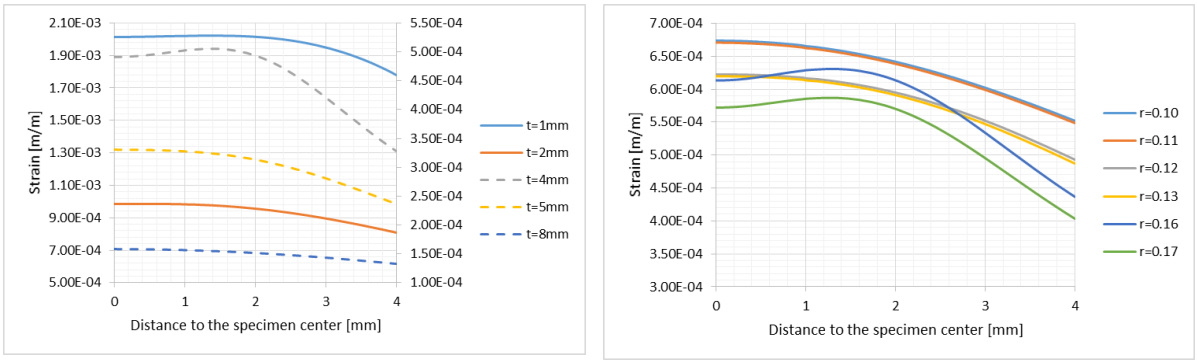

a) b)

Figure 6. Normal strain distributions on the specimen center: a) ratio r = 0.15 1, b) Specimen thickness t = 3 mm.

6. CONCLUSIONS

The Direct Multisearch algorithm was able to produce the Pareto Fronts for all of the analyzed specimen thickness. In a very complicated Finite Element problem the specimen geometries defined by eight active design variables were optimized using a DMS algorithm. Results were organized using both objective functions used, the maximum stress on the specimen center and the specimen reduced center thickness. Within the Pareto Front all the specimen geometries configurations are mathematically equal, therefore a full map for a specimen design recommendation was produced, based on the Renard Series of preferred number for the specimen thickness. It was possible to conclude that both the specimen elliptical arms fillet and center revolved spline are related with the specimen thickness and the specimen reduced center thickness and the specimen thickness ratio r. In fact the design variables that define the elliptical fillet are directly related with the specimen ratio, while the design variables that define the revolved spline are directly related with the ratio r. One can also see that the elliptical fillet will increase in size and become further away from the specimen center with the increase of the specimen center, while the revolved spline center radius will decrease with the increase of the ratio r. It was also possible to conclude that the maximum stress on the specimen center does not depends on the ratio r, and therefore the material manufacturing limitations can be overcome by choosing a higher specimen reduced center value without sacrificing the maximum stress level. As expected the maximum stress level decreases as the specimen thickness increases. Comparing the strain distribution on the specimen center, for different values of the ratio r, it is possible to conclude that the maximum strain difference on a radius of 1 mm around the specimen center will increase

with r, as the revolved spline geometry is changed.

REFERENCES

[1] a. Shanyavskiy, "Fatigue cracking simulation based on crack closure effects in Al-based sheet materials subjected to biaxial cyclic loads," *Eng. Fract. Mech.*, vol. 78, no. 8, pp. 1516–1528, May 2011.

[2] R. Sunder and B. V. Ilchenko, "Fatigue crack growth under flight spectrum loading with superposed biaxial loading due to fuselage cabin pressure," *Int. J. Fatigue*, vol. 33, no. 8, pp. 1101–1110, Aug. 2011.

[3] R. a Cláudio, M. Freitas, L. Reis, B. Li, and I. Guelho, "Multiaxial Fatigue Behaviour of 1050 H14 Aluminium Alloy by a Biaxial Cruciform Specimen Testing Method," *10th Int. Conf. Multiaxial Fatigue Fract.*, p. 1050, 2013.

[4] R. A. C. M. Freitas, L. Reis, B. Li, I. Guelho, V. Antunes, J. Maia, "In-plane biaxial fatigue testing machine powered by linear iron core motors," *Sixth Symp. Appl. Autom. Technol. Fatigue Fract. Test. Anal.*, p. ASTM STP 1571, 2013.

[5] R. Baptista, R. A. Claudio, L. Reis, I. Guelho, M. Freitas, and J. F. A. Madeira, "Design optimization of cruciform specimens for biaxial fatigue loading," *Frat. ed Integrità Strutt. (Fracture Struct. Integrity)*, vol. 30, pp. 118–126, 2014.

[6] Y. Hanabusa, H. Takizawa, and T. Kuwabara, "Numerical verification of a biaxial tensile test method using a cruciform specimen," *J. Mater. Process. Technol.*, vol. 213, no. 6, pp. 961–970, Jun. 2013.

[7] W. Müller and K. Pöhlandt, "New experiments for determining yield loci of sheet metal," *J. Mater. Process. Technol.*, vol. 60, no. I 996, pp. 643–648, 1996.

[8] E. Lamkanfi, W. Van Paepegem, and J. Degrieck, " ," *Polym. Test.*, vol. 41, pp. 7–16, 2015.

[9] T. Lagoda, E. Macha, and W. X. Będkowski, "Critical plane approach based on energy concepts: application to biaxial random tension-compression high-cycle fatigue regime," *Int. J. Fatigue*, vol. 21, pp. 431–443, 2000.

[10] V. Bonnand, J. L. Chaboche, P. Gomez, P. Kanouté, and D. Pacou, "Investigation of multiaxial fatigue in the context of turboengine disc applications," *Int. J. Fatigue*, vol. 33, no. 8, pp. 1006–1016, 2011.

[11] A. A. Zadpoor, J. Sinke, and R. Benedictus, "Experimental and numerical study of machined aluminum tailor-made blanks," *J. Mater. Process. Technol.*, vol. 200, pp. 288–299, 2008.

[12] A. A. Zadpoor, J. Sinke, and R. Benedictus, "Bendability of machined aluminium tailor-made blanks," *Int. J. Mater. Form.*, vol. 2, pp. 821–824, 2009.

[13] L. Leotoing, D. Guines, I. Zidane, and E. Ragneau, "Cruciform shape benefits for experimental and numerical evaluation of sheet metal formability," *J. Mater. Process. Technol.*, vol. 213, no. 6, pp. 856–863, Jun. 2013.

[14] E. Lamkanfi, W. Van Paepegem, J. Degrieck, C. Ramault, A. Makris, and D. Van Hemelrijck, "Strain distribution in cruciform specimens subjected to biaxial loading

conditions. Part 2: Influence of geometrical discontinuities," *Polym. Test.*, vol. 29, no. 1, pp. 132–138, Feb. 2010.

[15] E. Lamkanfi, W. Van Paepegem, J. Degrieck, C. Ramault, A. Makris, and D. Van Hemelrijck, "Strain distribution in cruciform specimens subjected to biaxial loading conditions. Part 1: Two-dimensional versus three-dimensional finite element model," *Polym. Test.*, vol. 29, no. 1, pp. 7–13, Feb. 2010.

[16] a. Makinde, L. Thibodeau, and K. Neale, "Development of an apparatus for biaxial testing using cruciform specimens," *Exp. Mech.*, vol. 32, no. 2, pp. 138–144, Jun. 1992.

[17] I. Guelho, L. Reis, M. Freitas, B. Li, J. F. A. Madeira, and R. A. Cláudio, "Optimization of Cruciform Specimen for a Low Capacity Biaxial Testing Machine," *10th Int. Conf. Multiaxial Fatigue Fract.*, 2013.

[18] I. O. for Standardization, "ISO 3, Preferred numbers — Series of preferred numbers," 1973.

[19] A. L. Custódio, J.F.A. Madeira, A. I. F. Vaz and L. N. Vicente. Direct Multisearch for multiobjective optimization. SIAM Journal on Optimization, 21(3):1109-1140, 2011.